Recent Progress of Mercury Lattice Clock in SIOM

Qixin Liu,[1,2,3] Ye Zhang,[1,2,3] Zexin Yu,[1,2,3] Jianfang Sun,[1,2] and Zhen Xu[1,2,3,*]
1 Shanghai Institute of Optics and Fine Mechanics, Chinese Academy of Sciences, Shanghai 201800, China
2 Key Laboratory of Quantum Optics, Chinese Academy of Sciences, Shanghai 201800, China
3 University of Chinese Academy of Sciences, Beijing 100049, China
Shanghai, China
* xuzhen@siom.ac.cn

***Abstract*—To realize a neutral mercury lattice clock, an experimental setup is in developing in SIOM. With two stable cooling lasers and a new vacuum system, an enhanced cold mercury atom source is implemented based on a two-dimensional magneto-optical trap (2D-MOT). By applying a hybrid frequency stabilization method and optimization of the 2D-MOT, about 1.3×10^6 cold mercury atoms are obtained with a loading rate of 1.0×10^6 atoms/s. And a high power injection-locked Ti:sapphire laser at 725 nm is developed for optical lattice at magic-wavelength.**

Keywords—Hg atom; optical lattice clock; laser cooling; DUV laser

I. INTRODUCTION

Nowadays, the advanced optical lattice clocks have reached a fractional uncertainty of 10^{-18} level which promote the researches of fundamental physics [1-2]. The mercury (Hg) optical lattice clock has been studied due to its lower sensitivity to the blackbody radiation and it is a good candidate to test the variation of fine-structure constant [3-5]. Meanwhile, as a secondary representation of the second in the International System of Units (SI), mercury plays an important rule on the redefinition of the SI second in the future [6-8].

As the basis of the Hg optical lattice clock, the MOT of mercury has been demonstrated by several groups [9-16]. To improve the performance of the clock, it's important to enhance the loading rate of cold mercury atom and reduce the dead time. Therefore, we developed the two-dimensional (2D) magneto-optical trap (MOT) [17] to enhance the cold atom production in the 3D-MOT. Two stable frequency-quadrupled DUV lasers at 253.7 nm are used [18] for the 2D-MOT and 3D-MOT respectively, and the frequency stabilization scheme is designed to conveniently control the laser frequency and to efficiently use the DUV power.

Here, we report the recent progress for the neutral mercury optical lattice clock developed in SIOM. We implement the experimental setup of the 2D-MOT plus 3D-MOT configuration with a frequency-stabilized DUV cooling laser system. About 1.3×10^6 atoms are loaded into the 3D-MOT for ^{202}Hg with a loading rate of 1.0×10^6 atoms/s [19]. In addition, an optical lattice laser is developed based on the watt-level narrow line-width injection-locked Ti:sapphire laser [20].

This work was supported by National Natural Science Foundation of China (11874371, 91436105 and 12104474) and Strategic Priority Research Program of the Chinese Academy of Sciences (XDB21030200).

II. THE EXPERIMENTAL SETUP

A. The vacuum system

The neutral mercury atom has a much higher vapor pressure at room temperature than the other metal atoms. To take its advantage on the high atom density in background vapor and to maintain a high vacuum in science chamber simultaneously, a two-chamber system is used to meet this requirement. The titanium vacuum chamber which is shown in Fig.1 is mainly composed of a 2D-MOT chamber and a science chamber. A differential pump tube with an inner diameter of 1.5 mm is used to maintain a high vacuum in the science chamber, meanwhile the 2D-MOT chamber has a relatively higher background pressure. Combined with a 40 L/s ion pump, the vacuum in the science chamber reaches to 2×10^{-10} Torr.

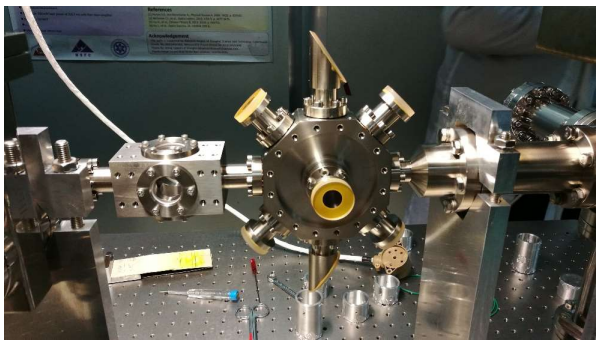

Fig.1 The apparatus of the 2D-MOT and 3D-MOT

An enhanced cold atom production is achieved with this two-chamber system. The 2D-MOT chamber has four UV fused silica (UVFS) windows with clear aperture of 20 mm and anti-reflection (AR) coating at 253.7 nm. On the science chamber, six AR-coated UVFS windows are used for laser cooling and fluorescence detection. The magnetic coils are mounted on the vacuum chamber to shorten the separation and reduce the power consumption, and the magnetic field gradient for 2D-MOT and 3D-MOT is 25 and 15 G/cm respectively.

In the next step, the interrogation of clock transition in the Lamb-Dick regime will be implemented in the vertical direction of science chamber with two Brewster windows for the optical access of optical lattice laser and clock laser.

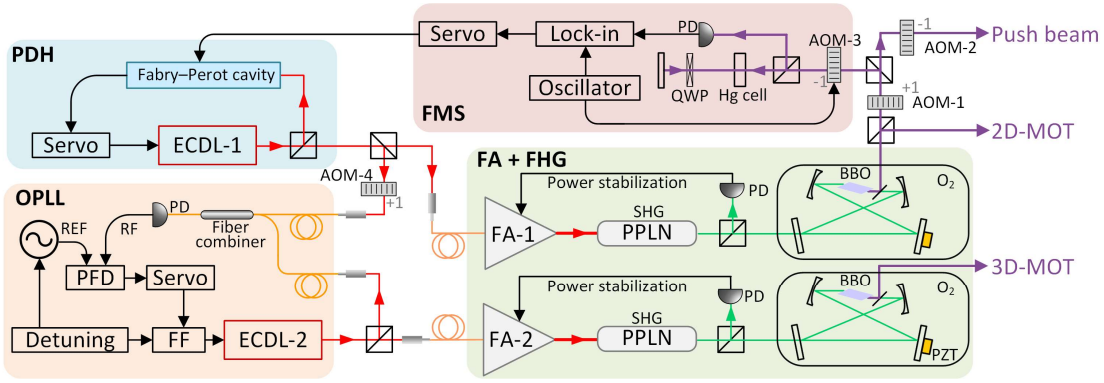

Fig. 2. Schematic diagram of the cooling laser system. BS, beam splitter; PDH, Pound-Drever-Hall; OPLL, optical phase locked loop; FF, feedforward circuit; FA, fiber amplifier; FHG, fourth harmonic generation; SHG, second harmonic generation; PD, photodiode; HR, high reflection mirror; FMS, frequency modulation spectroscopy.

B. Frequency-stabilized cooling laser system

The $^1S_0 - {}^3P_1$ transition at 253.7 nm is used for laser cooling of mercury atom with a natural line-width Γ of $2\pi\times1.27$ MHz and a saturated intensity of 10.2 mW/cm^2. To save the laser power and to individually tune the laser frequency, the cooling laser system with two frequency-quadrupled DUV lasers are employed, as shown in Fig.2. The DUV laser is fourth harmonic generated from a high-power fiber laser amplifier [18]. The seed lasers are two home-made external cavity diode lasers (ECDL-1 and ECDL-2) at 1014.9 nm. The ECDL-1 is frequency stabilized on a Fabry-Pérot cavity (FPC) by the Pound-Drever-Hall (PDH) method, and its line-width is narrowed to about 70 kHz. The typical error signal is shown in Fig 3 (a), which has a signal to noise ratio of 100. The output of fiber laser amplifier is converted to 507 nm laser via a single-pass PPLN crystal. The DUV laser at 253.7 nm is generated by a bow-tie cavity with a BBO crystal. To make the DUV laser more stable, an active power stabilization is used to reduce the power fluctuation of green laser. To ensure the continuously production of the cold atoms, the frequency doubling cavity is automatically relocked when the cavity is occasionally unlocked.

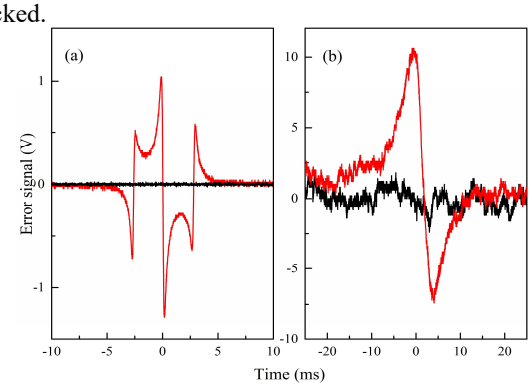

Fig. 3. The error signal of FPC locking (a) and SAS locking (b) when the laser frequency is scanned (red) and locked (black).

Most of the light from DUV-1 is send to the 2D-MOT, and about 10% optical power is split to pass through three AOMs for saturation absorption spectroscopy (SAS) and the push beam. DUV-1 is frequency locked by frequency modulation spectroscopy method (FMS) with a 91 kHz frequency modulation on AOM-3. Thus, the detuning of 2D-MOT beam (push beam) can be adjusted by AOM-2 and AOM-1 (AOM-3). The dispersive error signal from a lock-in amplifier is shown in Fig 3 (b). The line-width of the SAS is about 8 MHz, and the frequency fluctuation of DUV-1 laser is about 350 kHz in RMS, which is estimated from the error signal.

Full of the laser power from DUV-2 is sent to the 3D-MOT. The frequency of DUV-2 is controlled by an optical phase-lock loop (OPLL) [21] between two seed lasers at the 1014.9 nm. About 1 mW infrared light from ECDL-1 passes through AOM-4, and then beats with the light from ECDL-2. A phase frequency detector (PFD) is used to generate the error signal by comparing the phase difference between the reference signal (REF) and the beat note signal. The frequency difference between two ECDLs is normally several MHz. To reduce the time delay in PFD, the frequency of ECDL-1 is shifted with +80 MHz by AOM-4. In this laser system, the upper limit of detuning range depends on the maximum RF input frequency of the PFD chip and the lower limit depends on the polarity change of servo loop. Therefore, the detuning range of the OPLL is -80 to 400 MHz, which is rather larger than the required frequency variation in our experiment.

The detuning of 3D-MOT beams needs to be varied in several MHz within a typical switch time of 1 ms at different stage. To increase the bandwidth of the frequency tuning, a feedforward method is adopted in the OPLL by feed forward a synchronous signal to the current of ECDL-2. As a result, a 400 MHz laser frequency hopping of DUV-2 can be achieved within 1 ms.

To determine the long-term frequency stability between two ECDLs, the beat note frequency $\Delta\nu$ is measured by a frequency counter with a gate time of 0.1 s, and the frequency instability is shown Fig. 4. When ECDL-2 is free running, the frequency variation $\Delta\nu$ is as large as 160 MHz, which is mainly affected by the ambient temperature fluctuation. When ECDL-2 is locked on ECDL-1 by OPLL, the frequency instability is as good as the reference source. A voltage-controlled oscillator (VCO) and alternatively a direct digital synthesizer (DDS) are used to provide REF signal. When a VCO is used, the frequency

instability is several tens Hz. When it is replaced with a DDS, the frequency instability keeps decreased in 1000s, and it reaches 1.5×10^{-4} Hz at 1000 s.

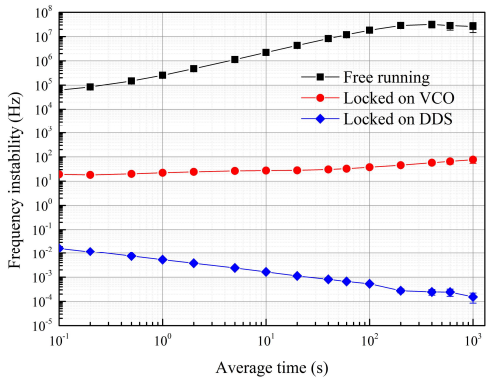

FIG. 4. Allan standard deviation of the beat note frequency when the ECDL-2 is free running (black), phase locked with a VCO (red) and a DDS (blue).

The linewidth of the DUV laser is measured by their beat note. It has a Lorentzian line-width of about 600 kHz, so the line-width of each DUV laser is estimated to be 300 kHz. To have a better frequency instability, a more stable REF is used in OPLL. However, in our experiment, both references satisfy our requirement and the VCO is adopted eventually due to its high-speed tunability for the time sequence.

III. Enhanced Production of Cold Mercury Atom

With this cooling laser system, the 2D-MOT of mercury atom is implemented and it results in the increasement on the loading rate and atom number of 3D-MOT. The detuning of the 2D-MOT beam, the push beam and the 3D-MOT beam will affect the atom number and the loading rate in the 3D-MOT. To obtain a stable atomic beam, the laser detuning of the 2D-MOT and push beam is optimized to -4Γ and -3.5Γ respectively. The detuning of 3D-MOT cooling laser is -8Γ in the loading stage and -1Γ in the fluorescence detection stage. Because of the tunability of our cooling laser system, these parameters can be optimized in the experiment.

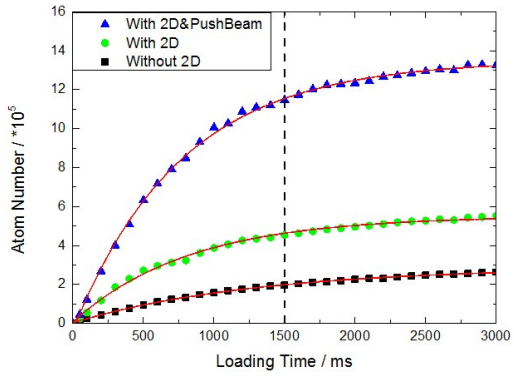

Fig. 5. Atom loading process of the 3D-MOT for ^{202}Hg atom when the push beam and 2D-MOT is on (blue triangle), only the 2D-MOT is on (green cycle) and 2D-MOT is absent (black square).

The atom loading process has been measured, as shown in Fig. 5 and it can be used to deduce the loading rate and loss rate [19]. As a result, with a 2D-MOT, the loading rate is increased about 3 times. With the cooperation of push beam and 2D-MOT, 8.4 times enhancement of the loading rate is achieved. Finally, about 1.3×10^6 ^{202}Hg atoms are loaded after 3 s, with a loading rate of 1×10^6 atoms/s.

IV. Optical Lattice Laser System

To develop the narrow-linewidth optical lattice laser at 362.5 nm, the injection-locked Ti:sapphire laser technology is adopted. The advantage of injection-locked Ti:sapphire laser is that both the narrow line-width and high power can be realized. However, it is hard to run an injection-locked Ti:sapphire laser at 725 nm because this wavelength is at the edge of gain profile of the Ti:sapphire crystal, and the gain at 725 nm is quite lower than that of gain peak at longer wavelength.

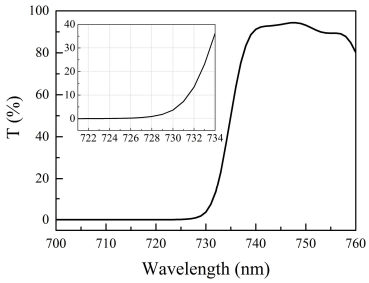

Fig.6 Transmission spectrum of long-pass-filter mirror. The reflection is > 99.8% at 725 nm and the transmission is > 90% above 740 nm.

A cavity mirror with a long-pass-filter coating is used in our Ti:sapphire cavity [20], and its transmission spectrum is shown in Fig. 6. With a sharp edge at 730 nm, this coating enlarges the optical loss at longer wavelength side. By suppressing the mode competition from the long wavelength side, the free-running wavelength of Ti:sapphire laser can be shorter, which makes it easier to injection locking at 725 nm. As a result, a watt-level injection-locked Ti:sapphire laser at 725 nm is achieved.

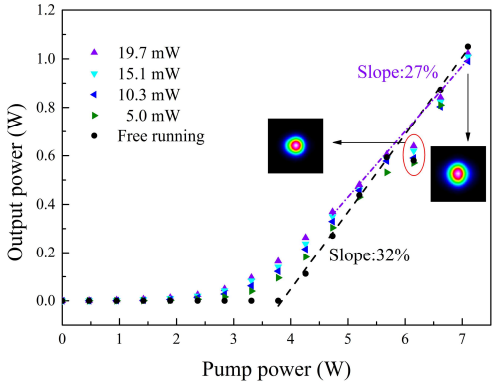

Fig. 7. Output power of the free-running and the injection-locked Ti:sapphire laser with different input power. The slope efficiency is 32% for the free-running Ti:sapphire laser (black dash line), and it is about 27% (purple dash dot line) for the injection-locked Ti:sapphire laser. The abnormal reduction of lase power at 6 W of pump power (in red circle) are caused by thermal effect, since the output beam appears different in the beam profile at this point.

This method effectively reduces the power requirement of the seed laser at 725 nm, and the Ti:sapphire laser can be injection-locked at higher output power. As shown in Fig. 7,

without the seed laser, the Ti:sapphire laser radiates 1 W of output power around 727 nm at a pump power of 7 W. When the Ti:sapphire laser is injection-locked on the seed laser, its output power is almost linearly increased by optical-optical slope efficiency of about 27% with pump power. A watt-level injection-locked Ti:sapphire laser can be obtained with an input seed power of as small as 5 mW.

The UV laser at 362.5 nm is generated by a frequency-doubling cavity with LBO crystal with output power of 210 mW. In the future, this optical lattice laser system will be used to load the cold atoms into a one-dimensional optical lattice. Vertical configuration of optical lattice will be adopted to reduce the probability of the tunneling between neighboring sites. To enhance the trap depth of the optical lattice, a build-up cavity will be installed outside of the vacuum chamber. We expect an intra-cavity power to be about 10 W, and it can be increased further by replacing the pump laser of the injection-locked Ti:sapphire laser.

V. CONCLUSIONS

The recent development of neutral mercury lattice clock is reported here, especially on the frequency-stabilized cooling laser system at 253.7 nm and the optical lattice laser system at 362.5 nm. With this cooling laser system, the enhanced cold atoms source of mercury is demonstrated with the 2D-MOT plus 3D-MOT configuration. Finally, about 1.3×10^6 ^{202}Hg atoms are loaded with a loading rate of 1×10^6 atoms/s. Based on these works, we expect to load the cold mercury atoms into the optical lattice, and interrogate the clock spectroscopy in Lamb-Dick regime. A mercury optical lattice clock will be fulfilled in the future.

REFERENCES

[1] M. Takamoto et al., "Test of general relativity by a pair of transportable optical lattice clocks," Nat Photonics, vol. 14, no. 7, pp. 411-415, July, 2020.

[2] T. Bothwell et al., "Resolving the gravitational redshift across a millimetre-scale atomic sample," Nature, vol. 602, no. 7897, pp. 420-424, February, 2022.

[3] J. J. McFerran et al., "Neutral Atom Frequency Reference in the Deep Ultraviolet with Fractional Uncertainty=5.7×10^{-15}," Phys Rev Lett, vol. 108, no. 18, pp. 183004, May 2012,

[4] K. Yamanaka, N. Ohmae, I. Ushijima, M. Takamoto, and H. Katori, "Frequency Ratio of ^{199}Hg and ^{87}Sr Optical Lattice Clocks beyond the SI Limit," Phys Rev Lett, vol. 114, no. 23, pp. 230801, June 2015.

[5] E. J. Angstmann, V. A. Dzuba, and V. V. Flambaum, "Relativistic effects in two valence-electron atoms and ions and the search for variation of the fine-structure constant," Phys Rev A, vol. 70, no. 1, pp. 014102, July 2004.

[6] M. Takamoto et al., "Frequency ratios of Sr, Yb, and Hg based optical lattice clocks and their applications," Cr Phys, vol. 16, no. 5, pp. 489-498, June 2015.

[7] R. Tyumenev et al., "Comparing a mercury optical lattice clock with microwave and optical frequency standards," New J Phys, vol. 18, no. 11, pp. 113002, November 2016.

[8] N. Ohmae, F. Bregolin, N. Nemitz, and H. Katori, "Direct measurement of the frequency ratio for Hg and Yb optical lattice clocks and closure of the Hg/Yb/Sr loop," Opt Express, vol. 28, no. 10, pp. 15112-15121, May 2020.

[9] H. Hachisu et al., "Trapping of neutral mercury atoms and prospects for optical lattice clocks," Phys Rev Lett, vol. 100, no. 5, pp. 053001, February 2008.

[10] M. Petersen et al., "Doppler-Free Spectroscopy of the S-1(0)-P-3(0) Optical Clock Transition in Laser-Cooled Fermionic Isotopes of Neutral Mercury," Phys Rev Lett, vol. 101, no. 18, pp. 183004, October 2008

[11] S. Mejri, J. J. McFerran, L. Yi, Y. Le Coq, and S. Bize, "Ultraviolet laser spectroscopy of neutral mercury in a one-dimensional optical lattice," Phys Rev A, vol. 84, no. 3, pp. 032507 September 2011,

[12] P. Villwock, S. Siol, and T. Walther, "Magneto-optical trapping of neutral mercury," Eur Phys J D, vol. 65, pp. 251-255, Novwmber 2011,

[13] C. Lytle, J. Paul, T.-H. Wu, and R. J. Jones, "Precision spectroscopy of the optical clock transition in laser cooled neutral Hg," in Frontiers in Optics 2014, Tucson, Arizona, 2014: Optica Publishing Group, in OSA Technical Digest (online), p. JTu3A.14.

[14] M. Witkowski et al., "Dual Hg-Rb magneto-optical trap," Opt Express, vol. 25, no. 4, pp. 3165-3179, February 2017

[15] Q. Lavigne, T. Groh, and S. Stellmer, "Magneto-optical trapping of mercury at high phase-space density," Phys Rev A, vol. 105, no. 3, pp. 033106, 03/15/ 2022,

[16] H. L. Liu et al., "Magneto-optical trap for neutral mercury atoms," Chinese Phys B, vol. 22, no. 4, pp. 043701, April 2013

[17] K. Dieckmann, R. J. C. Spreeuw, M. Weidemüller, and J. T. M. Walraven, "Two-dimensional magneto-optical trap as a source of slow atoms," Phys Rev A, vol. 58, no. 5, pp. 3891-3895, November 1998,

[18] Y. Zhang, et al. “A stable deep-ultraviolet laser for laser cooling of mercury atoms,” Optics & Laser Technology, vol. 139, pp. 106956 January 2021.

[19] Y. Zhang, Q. Liu, J. Sun, Z. Xu, and A. N. D. Wang, "Enhanced cold mercury atom production with two-dimensional magneto-optical trap," Chinese Phys B, in press.

[20] Q. X. Liu, J. F. Sun, Y. Zhang, and Z. Xu, "725 nm watt-level injection-locked continuous-wave Ti:sapphire laser for a mercury optical lattice clock," Appl Optics, vol. 60, no. 34, pp. 10750-10755, December 2021.

[21] L. Cacciapuoti et al., "Analog+digital phase and frequency detector for phase locking of diode lasers," Rev. Sci. Instrum. vol. 76, no. 5, pp. 053111, May 2005.